IEEE Open Journal of Vehicular Technology

Received 24 December 2025; accepted 8 January 2026. Date of publication 14 January 2026;
date of current version 30 January 2026. The review of this article was coordinated by Editor Lei Zhang.

Digital Object Identifier 10.1109/OJVT.2026.3653419

Spiking Neural Networks for Accurate and Efficient State of Health Estimation of Lithium-Ion Batteries Across Varying Temperatures

SLIMANE ARBAOUI [1], TEDJANI MESBAHI [1] (Senior Member, IEEE), THÉO HEITZMANN [1], MARWA ZITOUNI [1], AMEL HIDOURI [2], LAKHDAR MAMOURI [1], ALI AYADI [1], AHMED SAMET [1], AND ROMUALD BONÉ [1]

[1]INSA Strasbourg, ICube Laboratory UMR 7357 and CNRS, Université de Strasbourg, 67000 Strasbourg, France
[2]Institut Marey Maison de la Métallurgie (I3M), Université Bourgogne Europe, 21000 Dijon, France

CORRESPONDING AUTHOR: SLIMANE ARBAOUI (email: slimane.arbaoui@insa-strasbourg.fr).

This work was supported in part by the French National Research Agency (ANR) under Project ANR-22-CE92-0007-02 and in part by the European Union through the Horizon Europe program and the Innovation program under Grant GAP-101103667.

ABSTRACT Machine learning (ML) and deep learning (DL) have become essential tools in lithium-ion battery research, particularly for estimating the State of Health (SOH). However, conventional SOH estimation methods often rely on repeated charge/discharge cycles under strictly controlled laboratory conditions, limiting their applicability in real world scenarios. In this study, we present a comprehensive lithium-ion battery dataset developed by our team to support data driven approaches for battery diagnostics and predictive modeling. The dataset comprises nineteen lithium iron phosphate (LFP) cells with cycle lifetimes ranging from 500 to 2600 cycles and reflects realistic usage conditions, including non constant discharge currents and tests conducted at 25 °C, 35 °C, and 45 °C. To demonstrate the utility of this dataset, we used a brain inspired Spiking Neural Network (SNN) referred to as SpikeSOH, a neuromorphic model that uses sparse, time coded spikes to mimic biological neurons. This approach provides temporal precision while reducing energy consumption. Our results show that the SNN-based model achieves an average Mean Absolute Error (MAE) of 4.5%, while also outperforming conventional deep learning models in computational efficiency, with an average inference time of 3.55 μs and an average energy consumption of 0.36 mJ. These characteristics make the model particularly suitable for integration into energy constrained battery management systems. By providing a realistic, high quality dataset and demonstrating the advantages of energy efficient neuromorphic models, this work advances accurate and scalable SOH estimation methods, helping safer and more reliable deployment of lithium-ion batteries in both first life and second life applications.

INDEX TERMS Battery monitoring, lithium-ion batteries, LFP dataset, machine learning, spiking neural networks, state of health.

I. INTRODUCTION

Electric mobility is reshaping the global transportation landscape, driven by pressing climate concerns, rapid urbanization, and the need for sustainable alternatives to fossil fueled vehicles. As of 2024, the electric vehicle (EV) market has reached a valuation of 561 billion USD, with more than 40 million EVs in operation worldwide. In parallel, the global energy storage market is projected to exceed 241 billion USD by 2030, according to BloombergNEF, underscoring the strategic role of batteries in enabling the energy transition.

This rapid growth places increasing demands on EV battery management systems (BMS). Accurate, real time knowledge of critical indicators, such as State Of Charge (SOC), State

Of Health (SOH), and Remaining Useful Life (RUL), is essential not only to ensure safety but also to optimize driving range and reduce operational costs. Among the available technologies, lithium-ion batteries have emerged as the dominant choice due to their high energy density and long cycle life [1], [2], [3].

Lithium Iron Phosphate (LFP) batteries have attracted particular attention for applications that demand both safety and longevity. LFP exhibits exceptional thermal stability and resistance to thermal runaway, maintaining reliable performance even under high temperature or high stress conditions [4], [5]. Coupled with their long cycle life, low cost, and recent improvements in energy density and manufacturing efficiency [6], LFP batteries are ideally suited for electric mobility, renewable energy storage systems, and grid scale applications [7], [8], [9]. These attributes make LFP a strong candidate not only for first life applications but also for second life usage, reinforcing its central role in the transition toward sustainable, reliable, and cost effective energy storage solutions.

As battery technologies advance, there is a growing need for models that can process data quickly and efficiently on embedded BMS hardware. Traditional machine learning (ML) and deep learning (DL) models have demonstrated strong predictive capabilities for SOC and SOH [10]. However, their high computational requirements, reliance on floating point operations, and limited generalization to unseen conditions pose significant barriers to deployment in resource constrained embedded systems, where real time inference is crucial for safety and operational efficiency.

Spiking Neural Networks (SNNs) [11] offer a promising solution. Inspired by the brain's event driven processing, SNNs operate asynchronously and emit spikes only in response to significant stimuli. This sparse, temporally precise processing reduces energy consumption and allows for fast inference on embedded devices, making SNNs particularly suited for real time battery monitoring in BMS. Unlike conventional neural networks, SNNs encode information into spike trains, integrate signals over time, and fire only when the membrane potential crosses a threshold. Learning can be achieved using biologically inspired mechanisms such as spike timing dependent plasticity (STDP) or surrogate gradient methods that allow backpropagation despite the non differentiable nature of spikes [12].

However, two key challenges must be addressed for battery diagnostics: (i) encoding continuous, noisy signals into informative spike patterns, and (ii) training SNNs efficiently on large scale datasets to achieve robust performance across variable operational conditions. Meeting these challenges is essential for deploying models that are both accurate and capable of real time, low power operation, requirements that are increasingly critical as EVs become ubiquitous.

In this study, we focus on the accurate and fast prediction of internal battery metrics, with a particular emphasis on SOH, a key measure of a battery's charge storage capability relative to its rated capacity:

$$\mathrm{SOH}(\%) = \frac{C_n(t)}{C_n(0)} \times 100 \tag{1}$$

where $C_n(0)$ is the initial capacity (at 25 °C) and $C_n(t)$ the capacity at a given cycle index. This work provides three contributions:

1) We present a standardized, diverse, and representative dataset of cycling LFP cells, collected using real world driving protocols and tested across a wide range of operating temperatures. This open source dataset is publicly available and designed to support both physics based and data driven battery modeling approaches.
2) We introduce SpikeSOH, a lightweight SNN-based framework for SOH prediction, capable of real time, energy efficient inference on embedded BMS devices, addressing the growing need for fast and low power battery monitoring.
3) Our model uses only intrinsic battery measurements: voltage, current, and temperature, without any electrochemical modeling or external features, while maintaining consistent predictive performance across a broad range of ambient temperatures (25 °C, 35 °C, 45 °C), highlighting robustness and adaptability.

The remainder of this paper is organized as follows. Section II surveys related work on SOH estimation. Section III provides background on spiking neural networks. Section IV details the proposed methodology, including data generation protocols and the architecture of the SNN model. Section V presents the experimental results, and Section VI concludes the paper and outlines directions for future work.

II. RELATED WORK

SOH estimation is a fundamental task in battery management systems, as it enables early identification of degradation, thereby mitigating safety risks such as thermal runaway, performance loss, or even catastrophic failure resulting from aging induced faults. Traditional SOH estimation techniques are typically classified into three primary categories: physical-chemical models [13], [14], [15], electrical equivalent circuit models [16], [17], [18], and machine learning based methods.

While physical and electrical models benefit from interpretability and a deep connection to battery physics, they often require extensive domain expertise and complex parameterization. Moreover, these approaches may fail to adequately capture the intricate, nonlinear, and dynamic nature of battery aging, particularly under varying operating conditions [19].

In contrast, ML based approaches have emerged as powerful alternatives for SOH estimation. These methods infer degradation patterns directly from historical battery data, enabling accurate modeling without needing a complete understanding of the battery's internal electrochemical mechanisms [20]. In particular, artificial neural networks (ANNs) have demonstrated strong capabilities in capturing nonlinear relationships between input features such as voltage, current,

TABLE 1. Comparison of Recent Data-Driven SOH Estimation Works With a Focus on Embedded Deployment

Ref.	Model	Inputs	Embedded focus	Size (R/E)
Zhao et al. [34]	Hybrid deep neural network	V, Qc, ΔV, ΔQc	✗	R: ∼22 k params
Pandiaraj et al. [35]	Residual CNN + BiGRU	I, V, T	✗	R: ∼61.8 k params
Wang et al. [28]	Spiking neural networks	Full life cycle electrochemical impedance spectroscopy	✓	Not mentioned
Cai et al. [36]	Transformer–LSTM fusion	I, V, T, energy	✗	E: 0.5–2 MB
Arbaoui et al. [24]	Encoder–LSTM combination	I, V, and T	✗	R: ∼2.20 MB
Li et al. [37]	Bidirectional LSTM	Capacity time series until the present time point	✗	R: ∼2.28 MB
Zhang et al. [38]	Kolmogorov-Arnold networks + LSTM	Features from I, V, T	✗	Not mentioned
He et al. [39]	Multi scale Convolutional Attention Mechanism	I, V, T during charge	✗	Not mentioned
Roman et al. [40]	Classical ML pipeline	30 features from charge voltage and current curves	✗	R: >720 MB
Giazitzis et al. [29]	CNN + GRU combination	Electrochemical impedance spectroscopy curve	✓	R: 2.51 KB
Luan et al. [30]	Graph Attention Network + Bi-GRU	V and Q fragments extracted based on incremental capacity analysis on charging data	✓	R: 1.76 MB
Zhou et al. [31]	CNN (mobile U-Net / mobileNet)	I, V	✓	R: 27 k−95 k params
Bairwa et al. [41]	MLP, GRU, TCN, LSTM comparison	I,V, T during discharge	✗	E: 0.8–1.5 MB depending on model
Xiang et al. [32]	Transformer encoder with semantic embeddings	I, V, T	✓	Not mentioned
Nowacki et al. [33]	Lightweight 1D CNN	Raw voltage-capacity time-series data during short-duration (100s) current pulses	✓	Not mentioned

and temperature and the corresponding degradation states. Building on these foundations, more advanced deep learning architectures, such as Convolutional Neural Networks (CNNs) [21], [22], which excel in learning spatial hierarchies, and Long Short Term Memory (LSTM) networks [23], which are adept at modeling temporal dependencies, have further enhanced predictive accuracy in SOH tasks.

More recently, transformer based architectures have been introduced into the battery diagnostics landscape [24], [25]. By leveraging self attention mechanisms, transformers achieve improved performance in long range sequence modeling, making them particularly suitable for capturing the complex temporal evolution of battery degradation.

Despite their success, these models exhibit notable limitations. First, they lack biological plausibility, meaning they do not mimic the efficient and adaptive signal processing mechanisms observed in natural neural systems. As a result, they often struggle to generalize robustly when confronted with highly variable or noisy data, which is common in practical battery usage scenarios. Second, their reliance on floating point arithmetic and dense computation results in significant energy consumption, posing challenges for real time deployment in embedded BMS or edge devices [26], [27]. This issue is particularly critical in automotive and grid scale applications, where low latency, energy efficient, and scalable solutions are essential.

These limitations are clearly reflected in recent studies. Table 1 summarizes the majority of these works, highlighting model size, either in terms of the number of parameters or the total model size when reported, as well as whether runtime efficiency and deployability on embedded systems were considered. It is evident that only a few studies have addressed these practical aspects [28], [29], [30], [31], [32], [33]. Among them, the first two studies primarily relied on electrochemical impedance spectroscopy (EIS) data. In practice, EIS measurements require specialized impedance characterization equipment to evaluate battery impedance across a range of frequencies. However, due to the high cost and operational

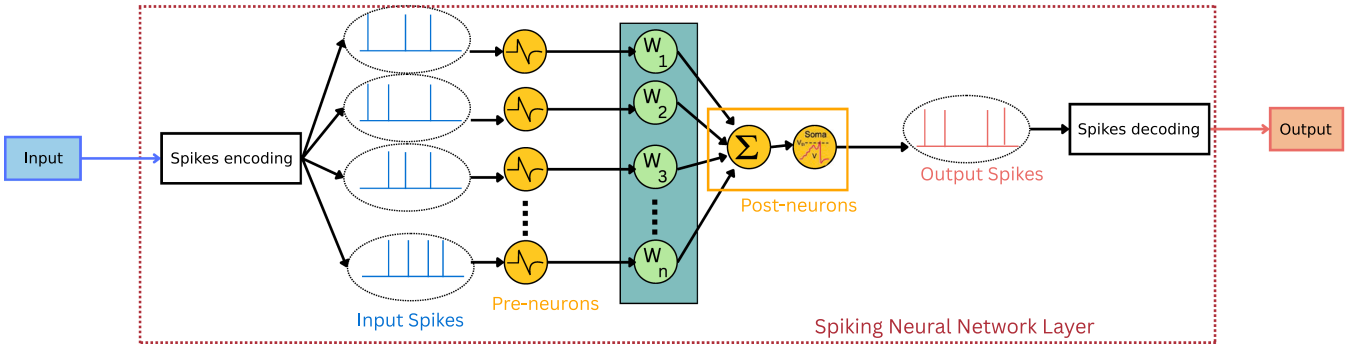

FIGURE 1. General architecture of an SNN, illustrating spike encoding, synaptic integration, LIF neuron processing, and spike decoding.

complexity of such equipment, many energy storage devices do not have the capability for real time impedance monitoring. As a result, approaches that rely on EIS data are often impractical for real world deployment, since the resulting models cannot be directly integrated into a BMS. The remaining studies focus on applying advanced data analysis techniques to extract meaningful information from the available datasets prior to model training, thereby reducing model complexity and improving performance.

By contrast, in this paper we present, to the best of our knowledge, the first SOH estimation model that explicitly accounts for both energy consumption and runtime efficiency using data directly provided by the BMS, without requiring complex preprocessing steps. Our approach leverages SNNs, which inherently model neuronal dynamics such as membrane potentials and synaptic delays. Unlike prior works that rely on specialized measurements such as EIS, our model operates directly on current, voltage, and temperature signals data that any BMS can provide in real time. This design makes our approach both energy efficient and readily deployable on embedded systems, enabling practical integration into real world battery management applications.

III. SPIKING NEURAL NETWORK MODEL

The basic properties and biodynamics of neurons can be modeled as the leaky integrate and fire (LIF) model [42]:

$$\tau_m \frac{dV(t)}{dt} = -(V(t) - V_{\text{rest}}) + R_m I(t)$$
$$\text{if } V(t) \geq \mathbb{S} \text{ then } \lim_{\substack{\alpha \to 0 \\ \alpha > 0}} V(t+\alpha) = V_r, \tag{2}$$

where $V(t)$ and V_{rest} stand for membrane potential and resting potential, respectively; τ_m stands for Membrane Time Constant (MTC), $I(t)$ stands for input current, R_m stands for leak resistance; $\mathbb{S}$ stands for firing threshold, and V_r stands for spike-after potential. This fully models the accumulation, leakage and firing processes of neuronal membrane potential. Assuming that there are n pre-neurons in the SNN layer, as depicted in Fig. 1, each pre-neuron sends an action potential $S_i(t)$ to the post-neuron at each time step, and the learnable weight corresponding to each pre-neuron is set to $w_1, w_2, \ldots, w_n$, then the SNN can be expressed as:

$$\tau_m \frac{dV(t)}{dt} = -(V(t) - V_{\text{rest}}) + \sum_{i=1}^{n} w_i S_i(t)$$
$$O(t) = 1\,(Firing)\, V(t^+) = V_r \text{ if } V(t) \geq \mathbb{S}$$
$$O(t) = 0\,(Silent) \text{ if } V(t) < \mathbb{S} \tag{3}$$

where $O(t)$ is the output of post-neurons, and O is a spiking train.

SNNs offer a biologically inspired computational framework centered around the LIF neuron model. Unlike traditional ANNs that encode information as continuous values, SNNs transmit data through discrete spike events, with key mechanisms such as membrane potential decay and threshold triggered firing capturing the temporal dynamics of real neurons. This allows SNNs to efficiently represent both spatial and temporal patterns. Furthermore, the sparse occurrence of spikes naturally reduces energy consumption. For example, based on measurements reported by Horowitz et al. [43] and Wang et al. [28], a 32-bit floating point multiply accumulate operation requires 4.6 pJ, whereas a floating point addition consumes only 0.9 pJ. Under comparable network parameters, with a single inference time step and a spike rate of 1, SNNs can achieve approximately fivefold lower energy usage than conventional ANNs, highlighting their potential for energy constrained applications.

Encoding continuous multivariate time series data into spike trains is a crucial step for applying SNNs to real world applications. Unlike traditional ANNs, which process data continuously, SNNs transmit information through discrete spikes, mimicking the behavior of biological neurons. This discrete nature allows SNNs to process data more efficiently, particularly in energy constrained environments. However, encoding multivariate time series data—such as current, voltage, and temperature in batteries, presents significant challenges. Improper encoding can lead to information loss, misaligned spikes, or inefficient representations that hinder the learning capacity of the SNN.

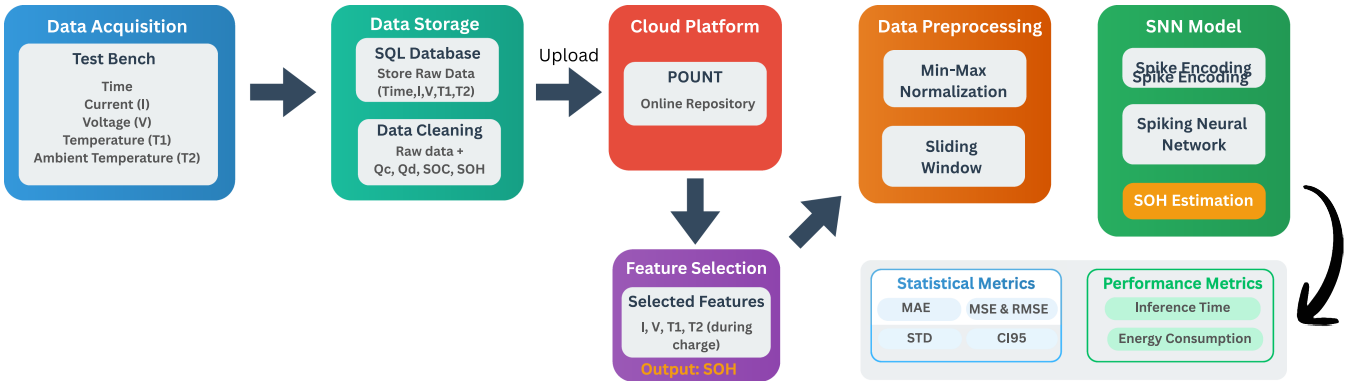

FIGURE 2. **Overview of the proposed approach.**

Several methods have been proposed to encode continuous signals into spike trains. *Rate coding* represents the magnitude of the input signal as the frequency of spikes within a given time window [44]. For multivariate data, each variable is typically encoded into a separate spike train. *Temporal coding* encodes information in the precise timing of individual spikes, effectively capturing temporal relationships between variables, but requiring precise synchronization [45]. *Sparse coding* represents input data using a small number of active neurons at any given time, which can improve efficiency but may require computationally intensive preprocessing [46].

IV. METHODOLOGY

Our approach, illustrated in Fig. 2, is structured around two key components: *data generation* and *model development*.

In the data generation phase, we establish an end to end experimental framework beginning with the configuration of the battery test bench, which involves defining cycling protocols, setting environmental conditions such as ambient temperature, and monitoring intrinsic battery signals, namely voltage, current, and temperature, while ensuring data consistency, traceability, and quality. The collected raw data is systematically processed, cleaned, and structured to support downstream modeling tasks, and the resulting dataset is made publicly available with comprehensive documentation and metadata annotations to promote reproducibility and collaboration. Building on this dataset, we develop a deep learning model based on SNNs, specifically designed for accurate and efficient SOH estimation. The model automatically learns temporal dynamics and degradation patterns directly from raw sensor signals without relying on prior electrochemical knowledge. Compared to different models that incorporate convolutional layers to extract local features, recurrent or attention based mechanisms to capture long term dependencies, and normalization strategies to enhance generalization, it demonstrates superior performance. The training process is rigorously validated under diverse operating conditions and multiple input–output configurations, with performance quantitatively assessed using established metrics, thereby confirming the model's robustness, practical relevance, and applicability to real world BMS.

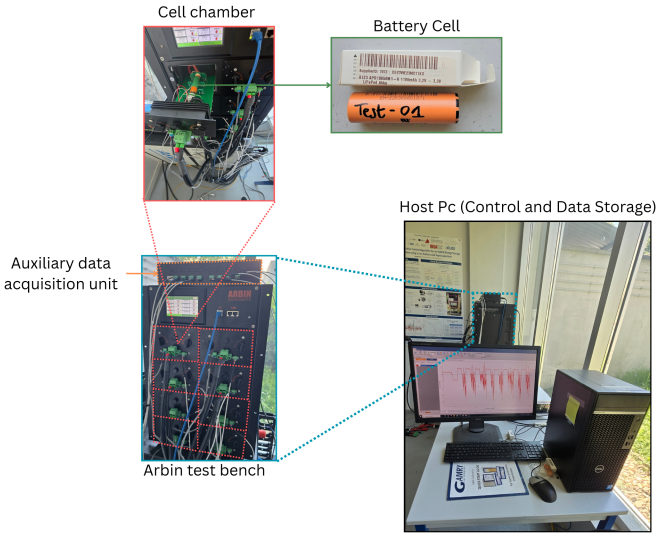

FIGURE 3. **Arbin battery test bench, including the thermal chambers, auxiliary data acquisition unit, LFP cell under test, and the host PC responsible for control and data storage.**

A. DATA GENERATION

The dataset was generated using a test bench developed by Arbin as shown in Fig. 3, that contains a general control unit linking all the measuring equipment and the computer. This unit receives battery cycling commands (current cycles, temperature setpoints...) from the computer and manages current distribution for cycling all cells. The setup has 8 climatic chambers providing thermal insulation and independent control of the ambient temperature inside. Each chamber is connected to the main unit by two cables supplying power for cell cycling, and two wires for measuring cell voltage throughout the test. An auxiliary unit measures the surface temperature of each cell, using *PT*100 probes for precision measurements. This unit then communicates this information to the main bench. These temperature data enable visualization of the thermal exchanges achieved by the battery during all phases of cycling, and in particular critical phases such as rapid charging or high dynamics during driving cycles. As each cell is cycled, the main unit transmits the measured

TABLE 2. Characteristics of LFP Cells [47]

Reference	APR18650M1B
Chemistry	LiFePO4
Nominal Voltage	3.3 V
Nominal Capacity	1.2 Ah
Charge Limit Voltage	3.6 V
Cut-off Voltage	2.0 V
Operating Temperatures	Ch :0°C-55°C Dch :-30°C-55°C
Cycle Life	>2000 cycles

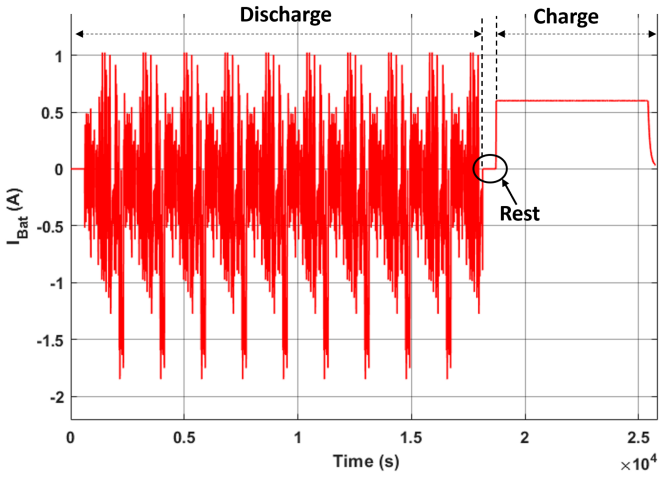

FIGURE 4. Current profile corresponding to the WLTC driving cycle.

current, voltage and temperature data to the computer for storage on a local server. A key feature of this bench is its eight thermally insulated chambers, each capable of independent temperature control ranging from 15 °C below ambient temperature up to 60 °C. We cycled 19 LFP cells, also known as LiFePO4, from LithiumWerks.[1] This chemistry remains widely used in electric vehicle batteries today, offering high energy density along with a broad range of conditioning and operating temperatures. The specific characteristics of the cells used in this study are outlined in Table 2.

Cells housed in the chambers undergo a repeated sequence consisting of a charging phase followed by a discharging phase. During the charging phase, cells are recharged according to two charging policies: *normal charging*, corresponding to the nominal charging current specified by the manufacturer, and *fast charging*, using the maximum allowable charging current. The discharging phase follows the Worldwide Harmonized Light Vehicles Test Cycle (WLTC) [48], as illustrated in Fig. 4.

The WLTC is a standardized driving cycle used to assess the performance of light duty vehicles [49], particularly electric vehicles, and to estimate their electric driving range [50].

[1]https://lithiumwerks.com/

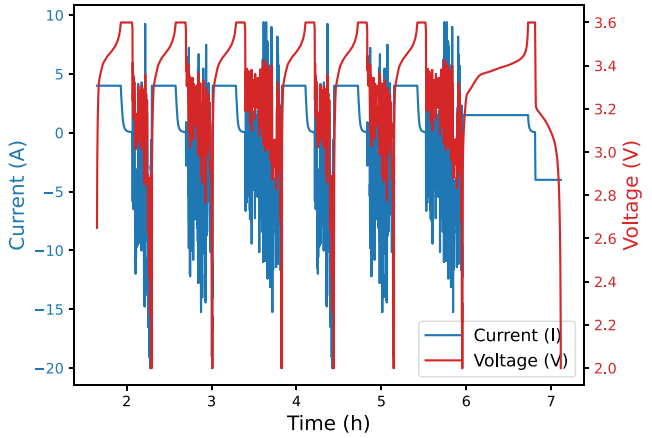

FIGURE 5. Current and voltage profiles during the first seven driving cycles under fast charging conditions at an ambient temperature of 25 °C.

These driving cycles are publicly available from the United Nations Economic Commission for Europe (UNECE).[2]

Using an electric vehicle traction model, the WLTC speed profiles were converted into corresponding power demand profiles. These were then normalized and transformed into current setpoint cycles suitable for cell level testing, enabling the replication of real world driving conditions. To accelerate battery aging, the current amplitudes were adjusted to align with the cells' discharge capacities.

To monitor the batteries' health, a dedicated health check cycle, consisting of a constant current charging and discharging phase, was carried out after every six driving cycles, as illustrated in Fig. 5. For each cell, we apply a data cleaning process to merge all files generated for that cell, as testing can occasionally be interrupted by events such as Windows updates. Once consolidated, the data is structured so that each row corresponds to a complete cycle. We then compute the charge capacity (Qc) and discharge capacity (Qd) by integrating the current over time during the charging and discharging phases, respectively. The SOC is calculated using the coulomb counting method [51], while the SOH is derived based on the capacity evolution over the cycles. As a result, for each cycle, we obtain the following features: current (I), voltage (V), temperature (T), charge capacity (Qc), discharge capacity (Qd), SOC and SOH. Table 3 provides additional details for each test, including the number of cycles, initial capacity, final SOH, and the applied charging policy.

The data was then uploaded to the *Plateforme OUverte Numérique Transdisciplinaire University of Strasbourg* (POUNT) platform[3] in two main formats: HDF5 and MAT. For each test, a description of the charge profile is provided, along with the ambient temperature at which the test was performed.

[2]https://unece.org/DAM/trans/doc/2012/wp29grpe/WLTP-DHC-12-07e.xls

[3]https://community.pages.unistra.fr/pount/pount-api/fr/pount/

TABLE 3. Overview of Cycling Test Data for Individual LFP Cells Under Different Charging Policies and Ambient Temperatures

Cell Name	Charging policy	Ambient Temp [°C]	Number of Cycles	Initial Capacity [Ah]	Final SOH	Mean duration per Cycle [min]
cell1-25	Fast charging	25	2756	1.21	0.44	38.43
cell2-35	Fast charging	35	2533	1.21	0.48	39.57
cell3-45	Fast charging	45	2291	1.22	0.50	39.18
cell7-25	Fast charging	25	2546	1.20	0.49	38.77
cell8-35	Fast charging	35	2337	1.21	0.66	40.38
cell9-45	Fast charging	45	2299	1.20	0.49	37.96
cell13-35	Fast charging	35	563	1.21	0.92	43.66
cell14-45	Fast charging	45	1935	1.21	0.87	68.80
cell15-45	Fast charging	45	2737	1.21	0.37	42.18
cell16-45	Fast charging	45	1663	1.21	0.82	68.73
cell17-45	Fast charging	45	1653	1.20	0.86	69.21
cell18-45	Fast charging	45	2547	1.21	0.50	42.52
cell19-45	Fast charging	45	2605	1.20	0.68	43.44
cell10-25	Normal charging	25	1570	1.19	0.89	61.80
cell11-35	Normal charging	35	2266	1.20	0.68	58.52
cell12-45	Normal charging	45	2427	1.20	0.57	56.57
cell4-25	Normal charging	25	1735	1.21	0.85	60.43
cell5-35	Normal charging	35	1936	1.22	0.75	60.43
cell6-45	Normal charging	45	1977	1.22	0.68	57.76

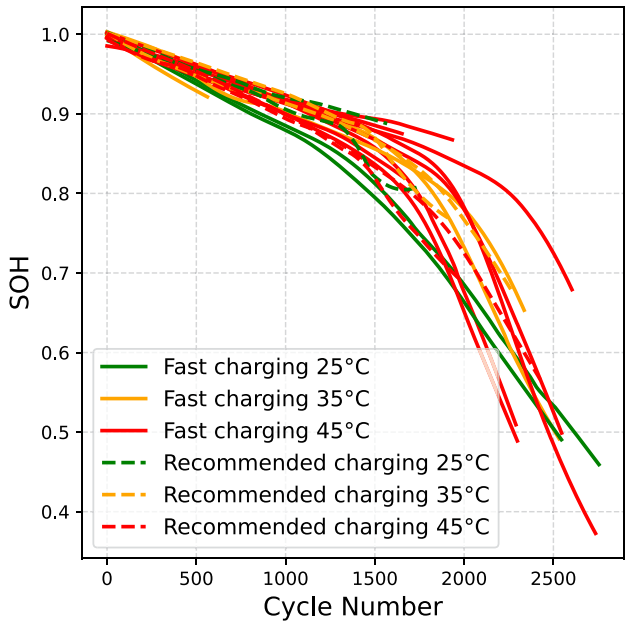

FIGURE 6. SOH evolution of the 19 battery cells subjected to different ambient temperatures (25 °C, 35 °C, and 45 °C) and charging current intensities, based on real world driving cycle simulations.

The objective of this experimental setup is to generate data enabling the analysis of two degradation factors: (i) the effect of battery temperature conditioning at three ambient temperatures (25 °C, 35 °C, and 45 °C), and (ii) the effect of charging speed, specifically the charging current intensity, on premature battery degradation. Driving cycles are used to replicate real world electric vehicle operation and to derive degradation curves, as shown in Fig. 6.

B. SPIKING NEURAL NETWORK FOR STATE OF HEALTH ESTIMATION

In this section, we employ the generated dataset to build a lightweight spiking neural network based model. SNNs are particularly well known for their low energy consumption, as their computations are based primarily on binary operations (0 or 1). Accordingly, it is crucial to prepare the data in a format compatible with spike based processing. This preparation step is both complex and critical, since the final model performance heavily depends on the quality of the encoding.

The proposed model takes as input the current, voltage, and temperature measurements recorded during the charging phase over X consecutive cycles and predicts the SOH values for the subsequent Y cycles, where $X \in \{1, 10, 20, 25\}$ and $Y \in \{1, 5, 10, 25, 50, 100, 200\}$. For both simplicity and computational efficiency, we limit the input sequence to a maximum of 25 cycles, which is sufficient to achieve accurate SOH estimations. This experimental design also enables a direct and fair comparison between our method and existing state of the art models.

We begin by applying min-max normalization to the data, ensuring that all features are scaled within the same range. The training dataset consists of three cells subjected to fast-charging profiles (Cells 1, 2, and 3) and tested under varying ambient temperatures. For evaluation, we selected all remaining cells, excluding those subjected to normal charging, to avoid introducing heterogeneity in the charge profile. Since the goal of this study is to model fast charge behavior specifically.

After normalization, a sliding window technique, similar to the method described in [52], is applied. This technique structures the inputs such that each sample corresponds to X consecutive cycles of data.

To transform the time series data into a sequence of spikes, it is essential to select an appropriate encoding method. It is important to note that as the number of charge-discharge cycles increases, the SOH of lithium-ion batteries gradually declines. This degradation is reflected in a reduction of the constant current (CC) charging time and a corresponding increase in the constant voltage (CV) charging time during the CCCV charging process, as illustrated in Fig. 7. These variations in current and voltage profiles must be carefully considered when designing the spike encoding strategy, which also justifies our choice of using only charging phase features.

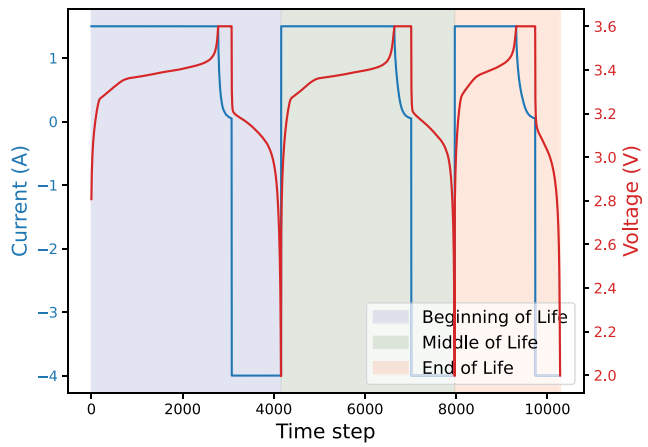

FIGURE 7. Current and Voltage profiles across battery lifecycle phases.

We apply binary encoding to the time series data based on the absolute differences between consecutive values. Specifically, we consider three key features from the input data current, voltage, and temperature and encode whether the differences between consecutive values exceed thresholds determined experimentally. If the difference surpasses the threshold, it indicates a significant change that needs to be captured, and we encode this as a 1. Otherwise, the change is considered negligible, and it is encoded as a 0. This approach enables us to precisely determine the duration of the CC and CV phases.

The input data is fed into a SNN designed for temporal signal processing. Each input sample $\mathbf{I} \in \mathbb{R}^{B\times X\times M\times F}$ consists of B batches of X historical cycles, with $M = 1500$ time points per charging phase and $F = 3$ features (current, voltage, temperature). The network includes two fully connected layers interleaved with LIF spiking layers to capture temporal and nonlinear dependencies, followed by a final linear projection and sigmoid activation to produce SOH predictions bounded between 0 and 1.

Training was performed with a batch size of 32, $N_{\text{hid}} = 1000$ hidden neurons, and an initial leak constant $\beta = 0.72$. Model parameters were optimized using the Adam optimizer with a learning rate of 5×10^{-4} and momentum coefficients $(\delta_1, \delta_2) = (0.9, 0.999)$. The mean absolute error was used as the loss function.

V. EXPERIMENTAL EVALUATION

A. IMPLEMENTATION

All experiments were conducted on a machine with an Intel Core i5 12th generation CPU, a NVIDIA GeForce RTX 3070 GPU with 8 GB of VRAM, 32 GB of RAM, and a 512 GB SSD. This machine provided the necessary computing power to train and test the models efficiently and effectively.

B. ERROR METRICS

To assess the performance of our proposed model, we utilized five widely adopted evaluation metrics: Mean Squared Error (MSE), Mean Absolute Error (MAE), Root Mean Squared Error (RMSE), Standard Deviation (STD) of errors, and the Confidence Interval (CI). These metrics evaluate the model's predictive accuracy over the full prediction horizon, consisting of Y predicted values, rather than individual points in isolation.

- *Mean Squared Error (MSE):* Depicted in (4), MSE measures the average of the squared differences between predicted and true values:

$$MSE = \frac{1}{n}\sum_{i=1}^{n}(\text{predicted\_value}_i - \text{observed\_value}_i)^2 \quad (4)$$

- *Mean Absolute Error (MAE):* As described in (5), MAE represents the average magnitude of the absolute errors between predicted and actual values:

$$MAE = \frac{1}{n}\sum_{i=1}^{n}|\text{predicted\_value}_i - \text{observed\_value}_i| \quad (5)$$

- *Root Mean Squared Error (RMSE):* Defined in (6), RMSE corresponds to the square root of the MSE, expressing the average prediction error in the same units as the original data:

$$RMSE = \sqrt{\frac{1}{n}\sum_{i=1}^{n}(\text{predicted\_value}_i - \text{observed\_value}_i)^2} \quad (6)$$

- *Standard Deviation (STD):* Measures the variability of the prediction errors, providing insight into the consistency of the model:

$$STD = \sqrt{\frac{1}{n}\sum_{i=1}^{n}\left((\text{predicted\_value}_i - \text{observed\_value}_i) - \bar{e}\right)^2},$$
$$\bar{e} = \frac{1}{n}\sum_{i=1}^{n}(\text{predicted\_value}_i - \text{observed\_value}_i) \quad (7)$$

- *Confidence Interval (CI):* Represents the range within which the true error is expected to lie with a given probability (commonly 95%):

$$CI = \bar{e} \pm z_{\alpha/2}\frac{STD}{\sqrt{n}}, \quad (8)$$

where $z_{\alpha/2}$ is the standard normal quantile corresponding to the desired confidence level (e.g., $z_{0.025} = 1.96$ for 95% CI).

C. RESULTS

To evaluate the effectiveness of the proposed model, namely `SpikeSOH`, we conducted a comprehensive comparative

TABLE 4. Architectural Configurations and Hyperparameters of Evaluated Models

Model	Architecture	Optimizer & Loss	Key Parameters
CNN-LSTM [53]	2 Conv1D BiLSTM + LSTM 2 Dense layers	Adam (lr=1e-3) Loss: MAE	Filters: 64, 128 (kernel: 5, 3) LSTM: 128, 64 Dropout: 0.2, 0.3
Encoder-LSTM [52]	Autoencoder + LSTM	Adam (lr=1e-4) Loss: MAE	Encoder: Flatten→256→128→100→(64×stepin) LSTM: 64, 32 AE epochs: 50
Tiny-CNN [33]	2 Conv1D 2 FC layers	Adam (lr=5e-4) Loss: MAE	Channels: 16, 32 Kernels: 15, 11 FC: 64
SpikeSOH	3 Linear layers 2 LIF neurons Spiking NN	Adam (lr=5e-4) Loss: MAE	FC: input→hidden→output→output LIF: Learnable β & threshold Time steps: 1 Output: Sigmoid activation
GRU-CNN [22]	CNN branch GRU branch Concatenation	Adam (lr=5e-4) Loss: MAE	CNN: 64 filters (kernel: 32) GRU: 256 hidden Fusion: 128→output

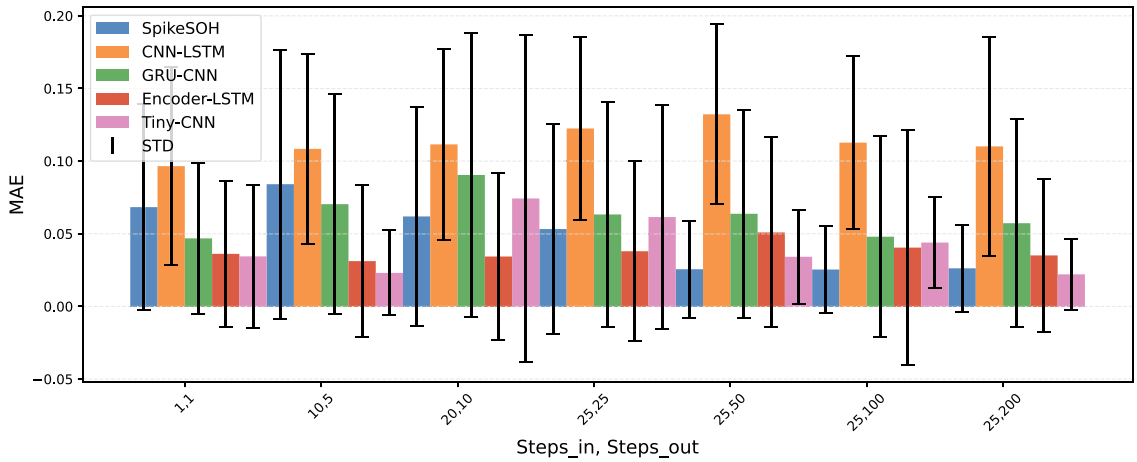

FIGURE 8. Mean Absolute Error and Standard Deviation for the five models across different window sizes.

study against four widely used deep learning based models: `Encoder-LSTM` [52], `CNN-LSTM` [53], `GRU-CNN` [22] and `Tiny-CNN` [33]. These baseline models were selected for their proven capabilities in capturing temporal dependencies and nonlinearities in battery degradation patterns. The architectural configurations and hyperparameters for all models are detailed in Table 4 and the comparative results are presented in Figs. 8 to 12, where models' performance was evaluated using common regression error metrics previously described.

The experimental results clearly demonstrate that `SpikeSOH` provides a balanced trade-off between accuracy and computational efficiency (especially when compared to the CNN model, which fails to achieve satisfactory accuracy when using only charging data), achieving an average MAE of 4.5%, an average MSE of 0.6%, an average standard deviation of 5% (the relatively higher standard deviation is expected, given the large test dataset and the inherent variability across individual cells), and a CI of 7.9×10^{-4}. A notable performance gap emerges when comparing SOH estimation using only a single cycle of input data versus using 25 cycles. With 25 input cycles, the model consistently achieves the best performance, even as the prediction horizon increases. This improvement is primarily due to the model's enhanced ability to recognize and exploit meaningful temporal patterns within the input data, particularly the durations of the CC and CV phases, which serve as strong indicators of the battery's degradation trajectory and overall condition throughout its lifecycle. In addition to accuracy, `SpikeSOH`

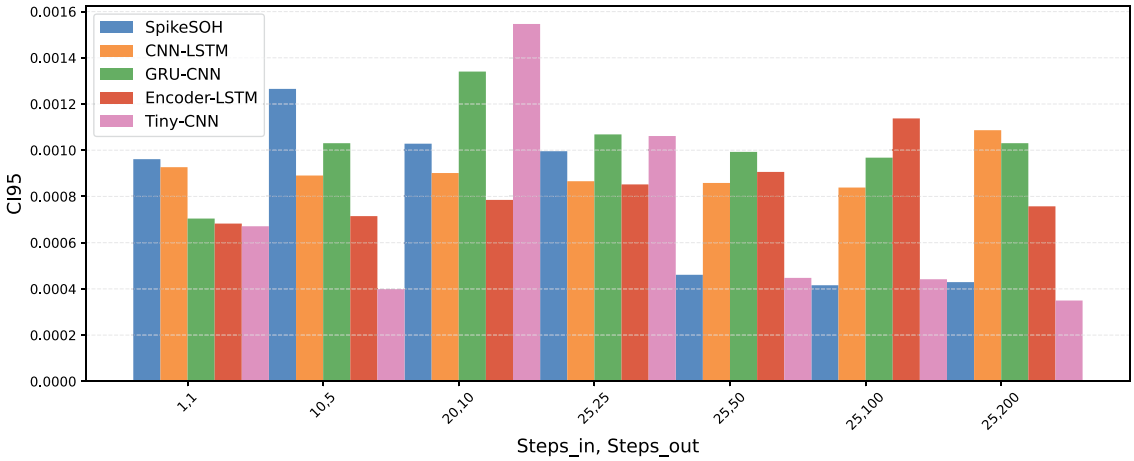

FIGURE 9. Confidence interval values for the five models across different window sizes.

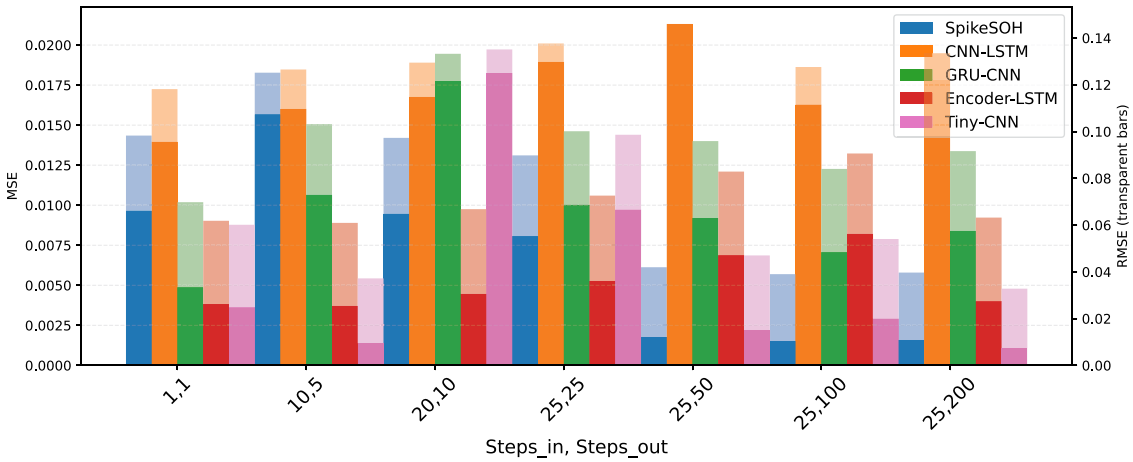

FIGURE 10. Mean Squared Error (MSE, solid) and Root Mean Squared Error (RMSE, transparent) for the five models across different window sizes.

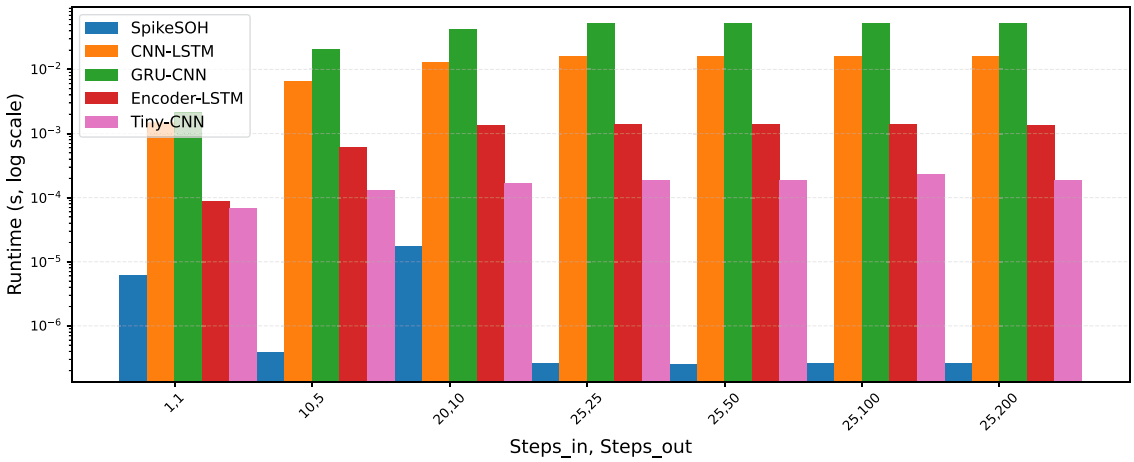

FIGURE 11. Model runtime (s) across different window sizes. Runtime is shown on a logarithmic scale to highlight small differences for fast running models.

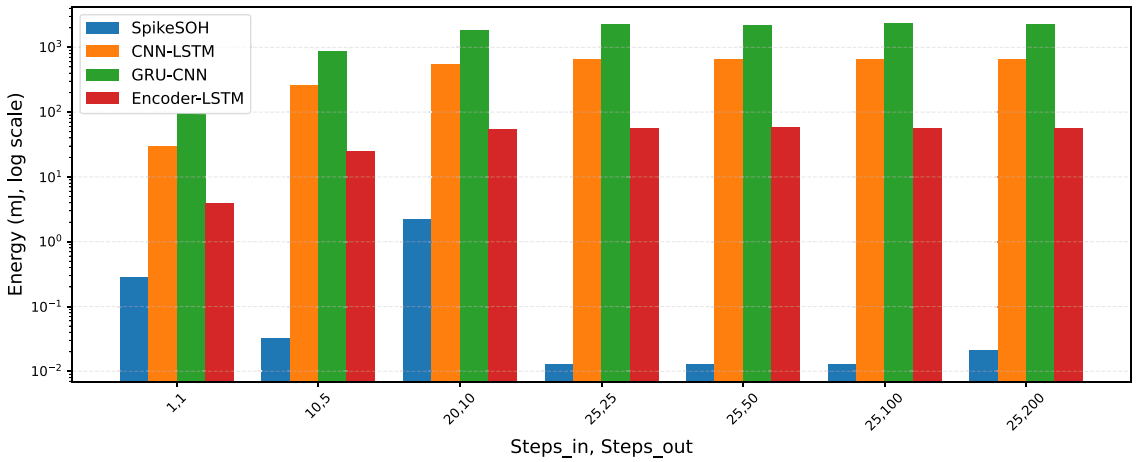

FIGURE 12. **Energy consumption (mJ) for each model across different window sizes.**

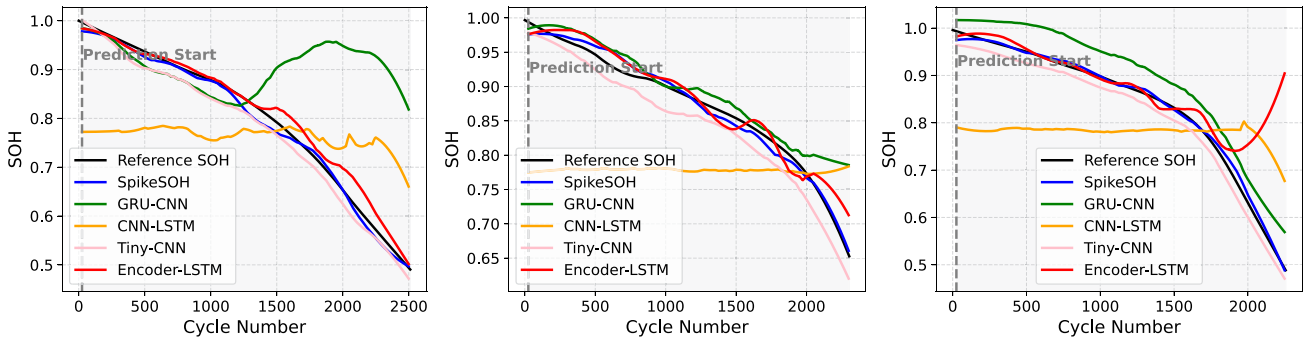

(a) 25°C (b) 35°C (c) 45°C

FIGURE 13. **Model performance at different ambient temperatures.**

demonstrates remarkable efficiency in both training and inference. Its event-driven architecture and reliance on simple arithmetic operations result in significantly lower computational requirements compared to conventional deep learning models, as illustrated in Fig. 12. The model provides predictions in an average time of 3.55 μs on GPU, 16 ms on CPU (single-threaded), and 40 ms on Raspberry Pi 5, making it highly suitable for deployment on embedded systems with limited resources. Moreover, `SpikeSOH` exhibits stable performance in terms of runtime and energy consumption, showing minimal variation across different input and output window sizes, unlike the other baseline models.

Furthermore, Fig. 13 demonstrates the robustness of `SpikeSOH` across a range of ambient temperatures, including 25 °C, 35 °C, and 45 °C. The corresponding SOH degradation patterns in Fig. 6 reveal the substantial impact of temperature on battery health trajectories, with `SpikeSOH` consistently delivering accurate predictions across all thermal conditions. Unlike physical/chemical models, which typically require separate calibrations or models for different thermal conditions, our approach maintains strong predictive performance without retraining. This generalizability highlights the model's suitability for real world applications, where batteries are subject to varying and unpredictable environmental conditions.

While the present study focuses on single-cell SOH estimation, `SpikeSOH` can be readily extended to battery modules and packs through strategic cell-level sampling approaches. Rather than monitoring every individual cell, which would be prohibitively expensive and computationally demanding in large-scale systems, the model can leverage measurements from a carefully selected representative subset of cells that capture the spatial variability in voltage, current, and temperature distributions across the module. This subset should be strategically positioned to reflect thermal gradients, electrical load distribution, and known weak points within the pack architecture.

Two implementation strategies are feasible for module-level SOH estimation. In the first approach, measurements from multiple representative cells can be processed as a multi-dimensional time series, with the input dimensionality scaled proportionally to the number of monitored cells and

their temporal data length. This unified model architecture directly learns inter-cell correlations and aging heterogeneity. Alternatively, independent instances of `SpikeSOH` can be deployed in parallel for each monitored cell, with individual SOH predictions subsequently aggregated through statistical methods such as weighted averaging (based on cell position or historical reliability) or ensemble fusion techniques. The parallel deployment strategy offers enhanced fault tolerance and interpretability, as cell-specific degradation patterns remain explicitly accessible. This scalability, combined with the model's demonstrated accuracy and thermal robustness, positions `SpikeSOH` as a practical and deployable solution for hierarchical SOH estimation in real-world multi-cell modules and large-scale battery packs, from automotive applications to grid-scale energy storage systems.

VI. CONCLUSION

This study introduced a high resolution lithium-ion battery dataset centered on LFP chemistries, designed to reflect real world operating conditions through heterogeneous charge/discharge protocols and multiple ambient temperatures (25 °C, 35 °C, 45 °C). To demonstrate its utility, we proposed `SpikeSOH`, a spiking neural network based model for accurate and energy-efficient SOH estimation. Leveraging event-driven processing, the model achieves real time, low power predictions, making it highly suitable for embedded battery management systems in EVs and other resource constrained platforms.

Experimental results highlight the effectiveness of SNNs in delivering robust and accurate predictions under varying operational conditions, while significantly reducing computational and energy requirements (achieving over 280× faster inference and 99.2% less energy used compared to conventional models). With the growing availability of neuromorphic hardware, such approaches hold strong potential to advance next generation battery monitoring systems.

Future work will systematically extend this research along four key directions. First, we aim to integrate the proposed methodology with emerging battery chemistries, including sodium-ion and lithium manganese iron phosphate, to assess generalizability across diverse electrochemical systems. Second, we plan to develop a more robust spike encoding strategy, enhancing resilience to measurement noise and improving model reliability in real-world conditions. Third, efforts will focus on improving model interpretability by leveraging the rich information contained in membrane potentials, providing deeper insights into the decision-making process of the spiking network. Finally, we will validate the framework on additional diagnostic tasks, such as state of charge estimation, under broader and more challenging operational scenarios, thereby demonstrating its versatility and practical applicability in advanced battery management systems.

VI. DATA AND CODE AVAILABILITY

The dataset used in this study is publicly available and can be accessed through the POUNT data repository. The source code used for model development and experiments is available on GitHub at the following repository: SNN model.

REFERENCES

[1] J. Lee, H. Sun, Y. Liu, and X. Li, "A machine learning framework for remaining useful lifetime prediction of li-ion batteries using diverse neural networks," *Energy AI*, vol. 15, 2024, Art. no. 100319.

[2] J. Morales, R. Trócoli, S. Franger, and J. Santos-Peña, "Cycling-induced stress in lithium ion negative electrodes: LiAl/LiFePO4 and Li4Ti5O12/LiFePO4 cells," *Electrochimica Acta*, vol. 55, no. 9, pp. 3075–3082, 2010.

[3] R. Konar, S. Maiti, N. Shpigel, and D. Aurbach, "Reviewing failure mechanisms and modification strategies in stabilizing high-voltage LiCoO2 cathodes beyond 4.55V," *Energy Storage Materials*, vol. 63, 2023, Art. no. 103001.

[4] Y. Yuan et al., "Influence of cathode materials on thermal characteristics oflithium-ion batteries," *Front. Chem.*, vol. 12, 2024.

[5] Y. Zeng, D. Chalise, S. D. Lubner, S. Kaur, and R. S. Prasher, "A review of thermal physics and management inside lithium-ion batteries for high energy density and fast charging," *Energy Storage Materials*, vol. 41, pp. 264–288, 2021.

[6] B. Chacko, and M. W, "A comprehensive investigation on the electrochemical performance, synthesis, modification, and recycling methods of LiFePO4 for sustainable future," *J. Energy Storage*, vol. 98, 2024, Art. no. 112851.

[7] S. Panchal et al., "Cycling degradation testing and analysis of a $LiFePO_4$ battery at actual conditions," *Int. J. Energy Res.*, vol. 41, no. 15, pp. 2565–2575, 2017.

[8] A. A. Kebede, T. Kalogiannis, J. Van Mierlo, and M. Berecibar, "A comprehensive review of stationary energy storage devices for large scale renewable energy sources grid integration," *Renewable Sustain. Energy Rev.*, vol. 159, 2022, Art. no. 112213, doi: 10.1016/j.rser.2022.112213.

[9] A. Tomaszewska et al., "Lithium-ion battery fast charging: A review," *eTransportation*, vol. 1, Aug., 2019, Art. no. 100011.

[10] J. Tao, S. Wang, W. Cao, P. Takyi-Aninakwa, C. Fernandez, and J. M. Guerrero, "A comprehensive review of state-of-charge and state-of-health estimation for lithium-ion battery energy storage systems," *Ionics*, vol. 30, no. 10, pp. 5903–5927, 2024.

[11] A. Tavanaei, M. Ghodrati, S. R. Saeed Kheradpisheh, T. Masquelier, and A. Maida, "Deep learning in spiking neural networks," *Neural Netw.*, vol. 111, pp. 47–63, 2019.

[12] E. O. Neftci, H. Mostafa, and F. Zenke, "Surrogate gradient learning in spiking neural networks: Bringing the power of gradient-based optimization to spiking neural networks," *IEEE Signal Process. Mag.*, vol. 36, no. 6, pp. 51–63, Nov. 2019.

[13] J. C. Burnset al., "Evaluation of effects of additives in wound li-ion cells through high precision coulometry," *J. Electrochem. Soc.*, vol. 158, no. 3, 2011, Art. no. A255.

[14] Y. Merla, B. Wu, V. Yufit, N. P. Brandon, R. F. Martinez-Botas, and G. J. Offer, "Novel application of differential thermal voltammetry as an in-depth state-of-health diagnosis method for lithium-ion batteries," *J. Power Sources*, vol. 307, pp. 308–319, 2016.

[15] T. Tatenda Makuwatsine and M. Singh, "State of charge (SoC) and state of health (SoH) estimation for electric vehicle battery," in *Proc. Int. Conf. Comput. Electron. Elect. Eng. Appl.*, 2024, pp. 1–6.

[16] X. Han, M. Ouyang, L. Lu, and J. Li, "Simplification of physics-based electrochemical model for lithium ion battery on electric vehicle. Part I: Diffusion simplification and single particle model," *J. Power Sources*, vol. 278, pp. 802–813, 2015.

[17] S. Nejad, D. T. Gladwin, and D. A. Stone, "A systematic review of lumped-parameter equivalent circuit models for real-time estimation of lithium-ion battery states," *J. Power Sources*, vol. 316, pp. 183–196, 2016.

[18] L. Mamouri, T. Pavot, and T. Mesbahi, "Parameter estimation for a generic na-ion battery model using the curve fitting approach," in *Proc. IEEE Veh. Power Propulsion Conf.*, 2024, pp. 1–5.

[19] S. Vigneshet al., "State of health (SoH) estimation methods for second life lithium-ion battery—Review and challenges," *Appl. Energy*, vol. 369, 2024, Art. no. 123542.

[20] Y. Liet al., "Data-driven health estimation and lifetime prediction of lithium-ion batteries: A review," *Renewable Sustain. Energy Rev.*, vol. 113, 2019, Art. no. 109254.
[21] J. Tian, R. Xiong, W. Shen, J. Lu, and F. Sun, "Flexible battery state of health and state of charge estimation using partial charging data and deep learning," *Energy Storage Mater.*, vol. 51, pp. 372–381, 2022.
[22] Y. Fan, F. Xiao, C. Li, G. Yang, and X. Tang, "A novel deep learning framework for state of health estimation of lithium-ion battery," *J. Energy Storage*, vol. 32, 2020, Art. no. 101741.
[23] H. Meng, M. Geng, and T. Han, "Long short-term memory network with Bayesian optimization for health prognostics of lithium-ion batteries based on partial incremental capacity analysis," *Rel. Eng. Syst. Saf.*, vol. 236, 2023, Art. no. 109288.
[24] S. Arbaoui, A. Samet, A. Ayadi, T. Mesbahi, and R. Boné, "Dual-model approach for one-shot lithium-ion battery state of health sequence prediction," *Array*, vol. 24, 2024, Art. no. 100367.
[25] A. H. Ardakani, S. A. Abdollahian, and F. Abdollahi, "NARX transformer: A dynamic model for leveraging multi-cycle data in long-term battery state of health estimation," *IEEE Trans. Instrum. Meas.*, vol. 73, 2024, Art. no. 2530908.
[26] G. Indiveri and S.-C. Liu, "Neuromorphic silicon neuron circuits," *Front. Neurosci.*, vol. 9, 2015, Art. no. 118.
[27] K. Roy, A. Jaiswal, and P. Panda, "Towards spike-based machine intelligence with neuromorphic computing," *Nature*, vol. 575, no. 7784, pp. 607–617, 2019.
[28] H. Wang, Y.-F. Li, and Y. Zhang, "Bioinspired spiking spatiotemporal attention framework for lithium-ion batteries state-of-health estimation," *Renewable Sustain. Energy Rev.*, vol. 188, 2023, Art. no. 113728.
[29] S. Giazitziset al., "TinyML models for SoH estimation of lithium-ion batteries based on electrochemical impedance spectroscopy," *J. Power Sources*, vol. 653, 2025, Art. no. 237568.
[30] W. Luan, H. Chen, and Y. Zhang, "State of health for lithium-ion batteries based on explainable feature fragments via graph attention network and bi-directional gated recurrent unit," *Sensors*, vol. 25, no. 19, 2025, Art. no. 5953.
[31] Q. Zhou, J. Zhao, and F. Li, "Battery state of health estimation and incremental capacity analysis for charging with general current profiles using neural networks," 2025, *arXiv:2502.19586*.
[32] Y. Xiang, T. Guo, and C. Zhang, "Semantically embedded end-to-end deep learning for battery energy storage system SoH estimation using field data," *SSRN Electron. J.*, 2025, doi: 10.2139/ssrn.5617138.
[33] B. Nowacki, J. Ramamurthy, A. Thelen, C. Tischer, C. L. Pint, and C. Hu, "Rapid estimation of lithium-ion battery capacity and resistances from short duration current pulses," *J. Power Sources*, vol. 628, 2025, Art. no. 235813.
[34] J. Zhao, D. Li, Y. Li, D. Shi, J. Nan, and A. F. Burke, "Battery state of health estimation under fast charging via deep transfer learning," *iScience*, vol. 28, no. 5, 2025, Art. no. 112235.
[35] P. Pandiaraj and S. Kumaran Vijayalakshmi Natarajan, "Optimized deep convolutional neural networks for SoC and SoH estimation in electric vehicles using orangutan algorithm," *J. Energy Storage*, vol. 134, 2025, Art. no. 118140.
[36] X. Cai and T. Liu, "State of health prediction for lithium-ion batteries using transformer–LSTM fusion model," *Appl. Sci.*, vol. 15, no. 7, 2025, Art. no. 3747.
[37] W. Li, N. Sengupta, P. Dechent, D. Howey, A. Annaswamy, and D. U. Sauer, "One-shot battery degradation trajectory prediction with deep learning," *J. Power Sources*, vol. 506, 2021, Art. no. 230024.
[38] Z. Zhanget al., "Advanced state-of-health estimation for lithium-ion batteries using multi-feature fusion and KAN-LSTM hybrid model," *Batteries*, vol. 10, no. 12, 2024, Art. no. 433.
[39] T. He and Z. Gong, "State of health estimation for lithium-ion batteries using a hybrid neural network model with multi-scale convolutional attention mechanism," *J. Power Sources*, vol. 609, 2024, Art. no. 234680.
[40] D. Roman, S. Saxena, V. Robu, M. Pecht, and D. Flynn, "Machine learning pipeline for battery state of health estimation," *Nature Mach. Intell.*, vol. 3, pp. 447–456, 2021.
[41] B. Bairwa, R. Gupta, and P. Jain, "Cycle-based state of health estimation of lithium-ion cells using MLP, GRU, TCN, LSTM," *Sci. Rep.*, vol. 15, 2025, Art. no. 37078.
[42] W. Gerstner and W. M. Kistler, *Spiking Neuron Models: Single Neurons, Populations, Plasticity*, Cambridge, U.K.: Cambridge Univ. Press, 2002.
[43] M. Horowitz, "1.1 computing's energy problem (and what we can do about it)," in *Proc. IEEE Int. Solid-State Circuits Conf. Dig. Tech. Papers*, 2014, pp. 10–14.
[44] W. Gerstner and W. M. Kistler, *Neuronal Dynamics: From Single Neurons to Networks and Models of Cognition*, Cambridge, U.K.: Cambridge Univ. Press, 2014.
[45] S. Thorpe, J. Gautrais, and R. V. Rullen, "Spike-based strategies for rapid processing," *Neural Netw.*, vol. 14, pp. 715–725, 2001.
[46] B. A. Olshausen and D. J. Field, "Sparse coding with an overcomplete basis set: A strategy employed by v1?," *Vis. Res.*, vol. 37, pp. 3311–3325, 1997.
[47] T. Heitzmann, A. Samet, T. Mesbahi, C. Soufi, I. J., and R. Boné, "SocHAP: A new data driven explainable prediction of battery state of charge," in *Proc. Int. Conf. Comput. Sci.*, 2023, pp. 463–475.
[48] DieselNet, "Worldwide harmonized light vehicles test procedure (WLTP)," 2024. Accessed: Oct. 17, 2024. [Online]. Available: https://dieselnet.com/standards/cycles/wltp.php
[49] M. Tutuianuet al., "Development of the world-wide harmonized light duty test cycle (WLTC) and a possible pathway for its introduction in the European legislation," *Transp. Res. Part D: Transport Environ.*, vol. 40, pp. 61–75, 2015.
[50] J. Lasocki, "The WLTC vs NEDC: A case study on the impacts of driving cycle on engine performance and fuel consumption," *Int. J. Automot. Mech. Eng.*, vol. 18, pp. 9071–9081, 2021.
[51] A. G. Stefanopoulou and Y. Kim, "10-System-level management of rechargeable lithium-ion batteries," *Rechargeable Lithium Batteries*, pp. 281–302, 2015, doi: 10.1016/B978-1-78242-090-3.00010-9.
[52] S. Arbaoui, A. Samet, A. Ayadi, T. Mesbahi, and R. Boné, "Data-driven strategy for state of health prediction and anomaly detection in lithium-ion batteries," *Energy AI*, vol. 17, 2024, Art. no. 100413.
[53] H. Xu, L. Wu, S. Xiong, W. Li, A. Garg, and L. Gao, "An improved CNN-LSTM model-based state-of-health estimation approach for lithium-ion batteries," *Energy*, vol. 276, 2023, Art. no. 127585.